Presynaptic NMDA receptors on mouse mossy fiber terminals mediate rapid BDNF release by ketamine and hydroxynorketamine

Irem L. Atasoy-Rodriguez[1], Kenneth W. Johnson[2], Kishan Patel[1], Haroon Arain[3], Syed Zaidi[3], Karl F. Herold[1], Teresa A. Milner[3], Hugh C. Hemmings Jr.[1,2], Jimcy Platholi[1,3#]

[1]Department of Anesthesiology, Weill Cornell Medicine, New York, NY, USA
[2]Department of Pharmacology, Weill Cornell Medicine, New York, NY, USA
[3]Feil Family Brain and Mind Research Institute, Weill Cornell Medicine, New York, NY, USA

[#]Corresponding author: jip2003@med.cornell.edu

Abstract

Enhancement of neuronal plasticity is a key determinant of the onset of antidepressant responses. Because brain-derived neurotrophic factor (BDNF)-dependent synaptic plasticity is essential for antidepressant efficacy, we examined whether fast-acting antidepressants directly trigger BDNF release. At antidepressant-relevant concentrations, ketamine and its metabolite (2R,6R)-hydroxynorketamine (HNK) induced BDNF secretion from mossy fiber terminals of granule neurons within minutes of application in rat hippocampal cultures. BDNF release required selective NMDAR signaling, as conditional genetic deletion of presynaptic NMDARs from granule neurons or from postsynaptic NMDARs from CA3 pyramidal neurons in acute mouse hippocampal slices, abolished BDNF exocytosis in response to both ketamine and HNK or selectively to HNK, respectively. Both compounds produced acute synaptic plasticity, reflected by gains and losses of CA3 dendritic spines without a net change in overall spine density. These findings reveal distinct, drug-specific NMDAR mechanisms at mossy fiber terminal–CA3 synapses that drive rapid BDNF release by fast-acting antidepressants.

Keywords: fast-acting antidepressants, brain-derived neurotrophic factor, presynaptic NMDA receptors, mossy fiber terminals, CA3 dendritic spines

Introduction

Ketamine, a widely used general anesthetic, has gained attention for its rapid and sustained antidepressant effects at low, subanesthetic doses[1]. Unlike conventional antidepressants, which show delayed onset and limited efficacy[2], a single ketamine infusion produces robust improvements in individuals with major depressive disorder[3, 4], including treatment-resistant cases[4, 5], within one hour [4, 6]. Antidepressant effects peak around 24 h and can persist for 7-14 days[4, 6], suggesting that ketamine engages both short- and long-lasting neuropharmacological mechanisms. Whether these effects arise from shared or distinct neural mechanisms remains unclear.

Enhancement of neuronal plasticity is a convergent requirement of both conventional and fast-acting antidepressants, with brain-derived neurotrophic factor (BDNF) emerging as a key mediator across drug classes[7, 8, 9, 10]. Transient, early elevations in BDNF (~30 minutes) occur in multiple brain regions[7, 11, 12, 13, 14], and are thought to precede behavioral improvement, and sustained elevations are not required for long-term antidepressant action[7]. Thus, the timing of BDNF release[7, 12, 13, 15] may be critical for determining onset of ketamine's effects.

Ketamine's antagonism of NMDA receptors (NMDARs)[7] aligns with pharmacological blockade of BDNF release by AMPARs and voltage-gated calcium channel inhibitors [12, 13]. However, the precise NMDAR populations that mediate ketamine-induced BDNF release remain unclear. Presynaptic NMDARs (preNMDARs) facilitate BDNF release from mossy fiber terminals[16], the large specialized boutons formed by dentate gyrus (DG) granule neurons onto CA3 pyramidal neurons and interneurons that regulate synaptic plasticity [17, 18]. The mossy fiber pathway contains the highest concentration of BDNF in the CNS [18, 19, 20], and although the mossy terminal-CA3 synapse has been implicated in actions of several antidepressants[21], its involvement in ketamine's mechanisms has not yet been directly examined.

Loss of dendritic spines, a structural correlate of chronic stress and depression[22, 23, 24, 25], is reversed by ketamine at multiple time points in both cortical [26, 27, 28] and hippocampal [29, 30] neurons, with *in vivo* restoration of spines in the medial frontal cortex persisting up to 2 weeks after treatment [31, 32]. Notably, ketamine restores cortical spines specifically at synapses functionally linked to depressive-like behavior, and spinogenesis is required for the maintenance, but not the emergence, of antidepressant responses [25, 33]. This synapse specificity, combined with its time

course[7, 11, 12, 13] and evidence that BDNF can prime adjacent dendritic sites for structural plasticity [34, 35], suggests that acute BDNF release drives rapid, targeted structural remodeling.

Using various rodent models, we show that preNMDAR signaling is required for the rapid release of BDNF from rodent mossy fiber terminals (MFTs) in response to low-dose ketamine and its metabolite, hydroxynorketamine (HNK). Using pharmacological interventions and conditional genetic deletion of presynaptic or postsynaptic NMDARs, we find that ketamine triggers BDNF release independently of NMDAR-mediated ion flux or of postsynaptic NMDARs, whereas HNK requires both presynaptic and postsynaptic NMDARs. Finally, we demonstrate that ketamine and HNK induce rapid, bidirectional structural plasticity in CA3 dendritic spines, reflected in dynamic increases and decreases in spine number without overall net changes in spine density, indicating a rapid redistribution rather than a net change in structural connectivity. These findings identify previously unrecognized hippocampal synaptic mechanisms involved in the onset of fast-acting antidepressant actions.

Results

Ketamine and hydroxynorketamine (HNK) rapidly induce BDNF release from mossy fiber terminals

Both ketamine and its metabolite HNK increase BDNF levels to produce antidepressant effects[12, 36, 37, 38]. To determine whether these fast-acting antidepressants directly trigger BDNF secretion from defined subcellular compartments[20, 39], we measured BDNF release from boutons and dendritic spines in dissociated rat hippocampal neurons expressing a pH-sensitive BDNF reporter fused to the C-terminus of BDNF (BDNF-SEP; Fig. 1). BDNF-SEP has been validated as properly processed, releasable, and biologically active [39]. Axonal and dendritic pools were confirmed using NH_4Cl alkalization at the end of each experiment (Fig. 1a). Acute application of ketamine (1 μM) and HNK (10 nM) evoked rapid BDNF release from presynaptic boutons within minutes and continued to drive asynchronous secretion throughout the 1 hr confocal imaging period (Fig. 1b-d and Supplementary Data: Video 1). Based on bouton size and morphology, these structures were identified as MFTs and further validated by immunocytochemistry (Fig. 1a and Supplementary Fig. 1). In contrast, neither ketamine nor HNK induced detectable BDNF release from dendritic spines within the same time window (Supplementary Fig. 2). Given that BDNF in the DG is essential for antidepressant efficacy[40, 41], and that the mossy fiber pathway projecting from the DG to CA3 (Fig. 1e) contains the highest BDNF concentration in the CNS[18], these findings reveal a previously unrecognized mechanism. To our knowledge, this is the first

demonstration that ketamine and HNK rapidly induce presynaptic BDNF release from MFTs, identifying a discrete hippocampal synapse engaged at the onset of fast-acting antidepressant action.

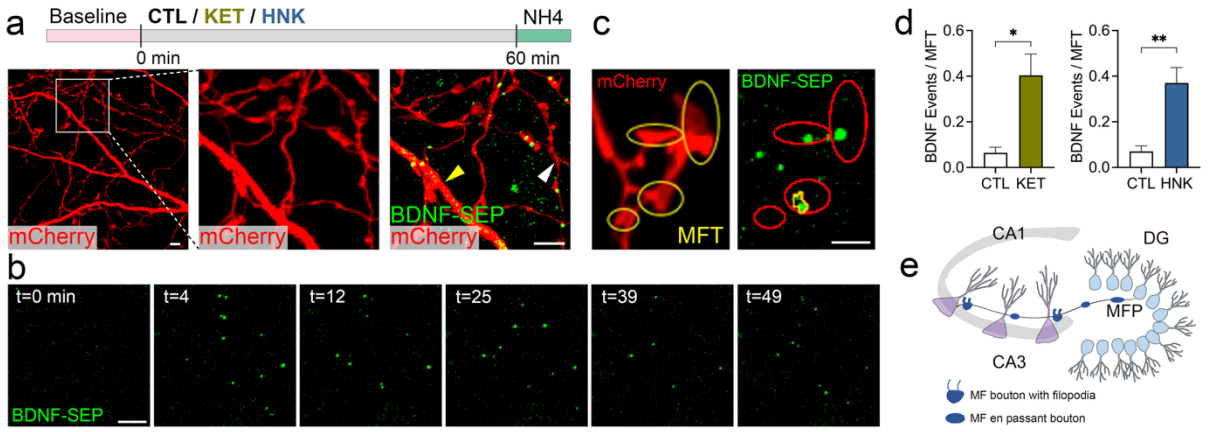

Fig.1. Rapid ketamine- and HNK-evoked release of BDNF from hippocampal mossy fiber terminals. (**a**) Rat hippocampal neurons (21 DIV) transfected with BDNF-SEP and mCherry were perfused with 1μM ketamine, 10nM HNK, or control buffer and imaged as indicated (top). Representative mCherry image of a control neuron showing dendritic arbors and axons (left). Inset: dendritic segment and single boutons before (middle) and after (right) NH_4Cl alkalinization, revealing BDNF-SEP pools in axons (white arrowhead) and dendrites (yellow arrowhead). (**b**) Representative images of single BDNF exocytotic events (green dots) before (t=0) and after (t=4-49) ketamine application with individual BDNF release events selectively arising from mossy fiber terminals (MFTs) chosen for analysis (**c**, circles). (**d**) Quantification of BDNF exocytosis showing increased release following ketamine or HNK treatment (*$p < 0.05$ and **$p < 0.01$; Student unpaired *t*-test). (**e**) Schematic of the hippocampal mossy fiber pathway (MFP) illustrating dentate gyrus (DG) granule neurons with their *en passant* boutons and mossy fiber boutons synapsing onto CA3 pyramidal neurons. Data represent mean ± SEM, n = 5-10 cells and 302-825 MFTs selected for each condition. Scale bars: 5 μm (**a**, **b**) and 2 μm (**c**).

NMDAR antagonism and presynaptic GRIN1 deletion reduce mossy fiber BDNF release induced by ketamine and HNK

Regulation of ligand- and voltage-gated channels[1, 12, 13], including both direct and indirect modulation of NMDARs[7, 42, 43, 44, 45, 46], has been proposed to converge on increases in BDNF levels that drive synaptic plasticity required for antidepressant efficacy. At mossy fiber synapses,

preNMDARs facilitate BDNF release underlying synapse-specific forms of plasticity[16], likely supported by their distinct subunit compositions[47, 48, 49] that enable both ionotropic and metabotropic signaling[50, 51, 52, 53, 54]. To verify NMDAR localization at MFTs, we performed pre-embedding immuno electron microscopy in mouse dorsal hippocampus[55] using a selective antibody against the GluN3A subunit[56, 57, 58] (Fig 2 a-c). Silver-intensified immunogold (SIG) particles for GluN3A were significantly enhanced on presynaptic MFTs relative to postsynaptic CA3 dendritic spines (Fig. 2d), confirming robust presynaptic expression. We next asked whether NMDAR signaling contributes to rapid BDNF release induced by ketamine. Hippocampal neurons were preincubated (3 min) with either the noncompetitive NMDAR antagonist MK-801 (10 μM) or the competitive antagonist APV (50 μM) before ketamine application. APV abolished ketamine-evoked BDNF release (Fig. 2e), demonstrating that glutamate binding is required for this acute effect. In contrast, MK-801, an open channel blocker, failed to prevent ketamine-evoked BDNF release, even at saturating concentrations, and MK-801 alone did not elicit detectable BDNF release (Fig. 2f) despite its reported short-acting antidepressant properties[59]. These results indicate that ketamine-driven BDNF release sites rely on competitive NMDAR antagonism and is independent of NMDAR-mediated ion flux.

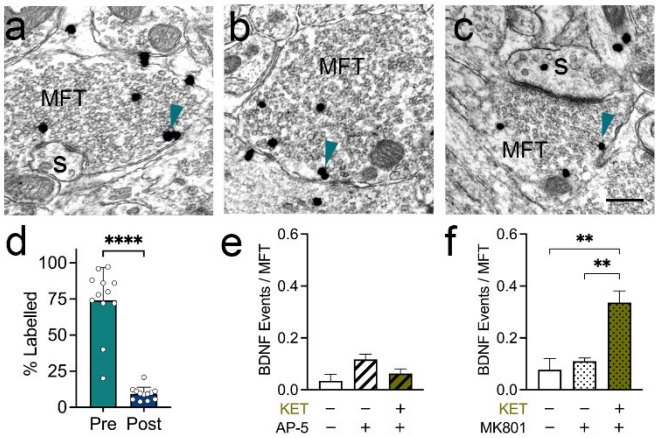

Fig. 2. Anatomical and functional evidence for NMDAR regulation by ketamine and HNK. (**a-c**) Electron micrographs showing GluN3A SIG labeling (black dots) of mossy fiber terminals (MFTs; **a, b**) and dendritic spines (S; **c**). SIG particles were observed predominantly on or near (arrows) the plasma membrane in MFTs. (**d**) Quantification of GluN3A SIG particles demonstrating greater GluN3A expression in MFTs (Pre) compared to dendritic spines (Post). Data for 50 GluN3A-labeled MFTs from randomly selected micrographs was obtained from 12 mice (6 males and 6 females) with each data point representing one animal; n = 432 profiles in presynaptic profiles; n

= 124 postsynaptic profiles). Data expressed as mean % labelled ± SEM (****$p < 0.0001$; Student unpaired *t*-test). Scale bar, 300 nm. (**e, f**) Quantification of BDNF exocytosis from MFTs showing that ketamine-evoked release is inhibited by preincubation with APV (50 μM) (**e**) but not MK-801 (10 μM) (**f**). **$p < 0.01$; one-way ANOVA. Data represent mean ± SEM, n = 3-7 cells and 222-596 MFTs analyzed per condition.

Because bath-applied antagonists block both axonal and dendritic NMDARs, we selectively deleted *GRIN*1 from DG granule neurons in *Grin1*^{flox} mice to test the specific contribution of preNMDARs. Cre-dependent mice (postnatal days 23-35) were injected unilaterally into the DG with AAV5-CaMKII-mCherry-cre and AAV-DJ-DIO-BDNF-pH to selectively delete *Grin1* and express BDNF-pH, respectively (Fig. 3a). Wild-type mice receiving the same viral injections served as controls. Robust expression of pHluorin (GFP) and mCherry in DG granule neurons and MFTs was confirmed in acute hippocampal slices four weeks after injection (Fig. 3b-d) and only acute slices with strong expression of both were used.

Using two-photon (2P) imaging, we found that ketamine (20 μM) and HNK (10 μM), concentrations shown to release BDNF (Fig. 3) and modulate hippocampal plasticity in cultured neurons and slices[60, 61], produced a marked reduction of BDNF release from MFTs in acute slices from *Grin1*-deleted mice after 5 minutes of treatment (Fig. 3e-h). Together, these findings demonstrate that NMDAR signaling, particularly in DG-derived mossy terminals, is necessary for rapid release of BDNF by ketamine and HNK.

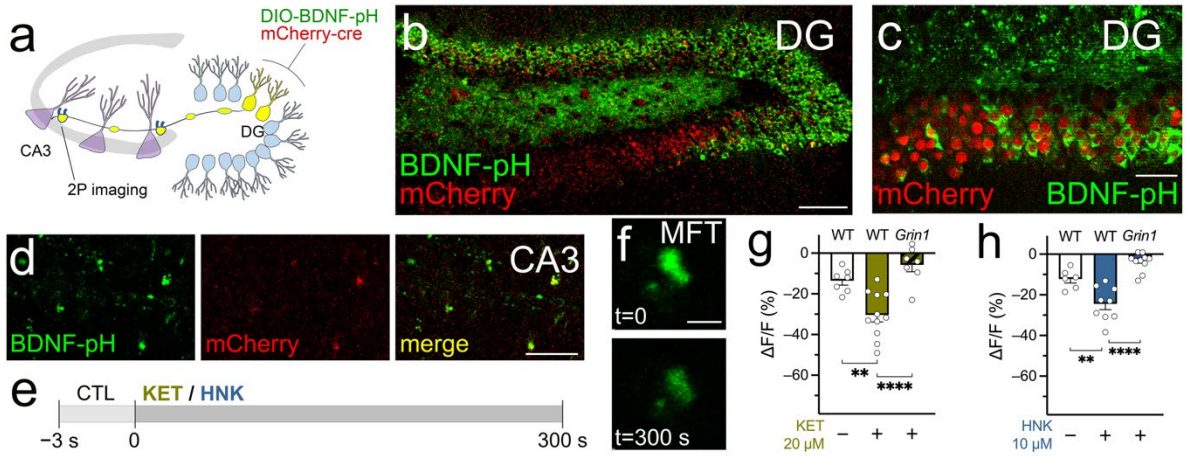

Fig. 3. preNMDARs are required for ketamine- and HNK-evoked BDNF release from mossy fiber terminals. (**a**) Schematic illustrating viral transduction of DG granule neurons with mCherry (red)

and BDNF-pH (green), resulting in co-labeling of MFTs at imaging sites in CA3 (yellow). (**b-d**) Representative images from acute hippocampal slices from *Grin1*^{flox} mice showing robust mCherry-cre expression (red; deleting GluN1 and enabling Cre-dependent BDNF-pH expression) in DG (**b, c**) and merged BDNF-pH + mCherry labeling in MFT in CA3 (**d**). (**e**) Experimental timeline showing baseline recordings in ACSF followed by perfusion with 20 μM ketamine or 10 μM HNK. (f) Representative images of BDNF-pH fluorescence in MFTs at baseline (t = 0) and after 300 s of ketamine exposure, showing decreased fluorescence corresponding to BDNF release. (**g, h**) Quantification of BDNF release from MFTs demonstrating that ketamine-evoked (**g**) and HNK-evoked (**h**) BDNF secretion is abolished in slices lacking NMDAR function in DG granule neurons. (**p < 0.01, ****p < 0.0001; one-way ANOVA with Tukey *post hoc* test). Data are mean ± SEM, n = 6-7 animals and 7-11 slices per condition. Scale bars:100 μm (**b**), 30 μm (**c, d**), and 5 μM (**f**).

NMDARs on postsynaptic CA3 neurons contribute to HNK-evoked, but not ketamine-evoked, BDNF release

To test whether dendritic NMDARs participate in ketamine- and HNK-induced BDNF release, we repeated the above experiments with conditionally deleted *Grin1 from* CA3 pyramidal neurons in *Grin1*^{flox} mice. These Cre-dependent mice were injected unilaterally with AAV5-CaMKII-mCherry-cre into area CA3 at postnatal days 23-35 to restrict *Grin1* deletion to postsynaptic compartments receiving mossy fiber input. Because CA3 pyramidal cell bodies lie in close proximity to DG neuron axons, complete avoidance of retrograde viral spread is not technically feasible, raising the possibility of partial presynaptic knockdown. To distinguish presynaptic from postsynaptic contributions, we simultaneously injected a non-Cre dependent AAV-DJ-BDNF-pH into CA3 to express BDNF-pH independently of *Grin1* status (Fig. 4a). This strategy yielded three fluorescent readouts: deletion of *Grin1* (mCherry; red); expression of BDNF-pH (pHluorin; green); and expression of BDNF-pH with *Grin1* deletion (mCherry + pHluorin; yellow) (Fig. 4b). To ensure BDNF fluorescence measurements reflected release from MFTs synapsing onto CA3 neurons lacking postsynaptic *Grin1* deletion, analyses were restricted to slices exhibiting strong mCherry expression in CA3 cell bodies but pHluorin-only expression in MFTs (Fig 4c). Under these conditions, ketamine (20 μM) evoked presynaptic BDNF release, indicating that somatodendritic NMDARs in CA3 are not involved in acute ketamine actions. In contrast, HNK-evoked (10 μM) BDNF release was significantly reduced in slices lacking postsynaptic NMDARs (Fig. 4d, e).

These results indicate that HNK, but not ketamine, requires postsynaptic NMDAR signaling to drive rapid BDNF release at mossy fiber-CA3 synapses.

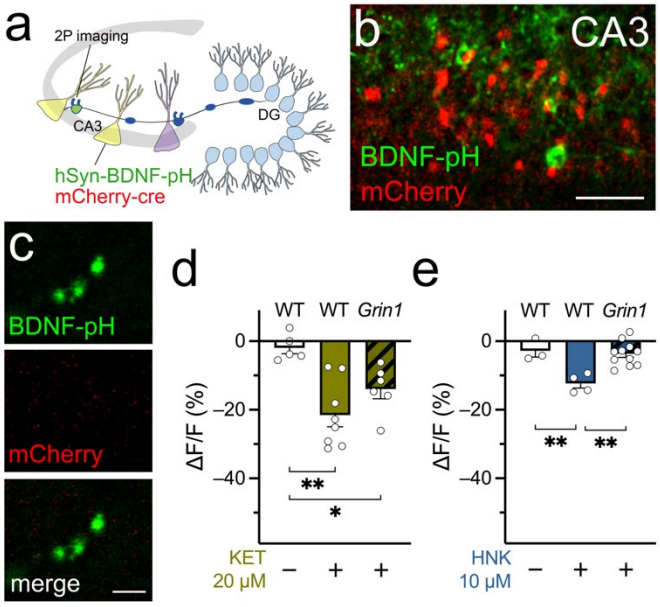

Fig. 4. Postsynaptic NMDARs are required for HNK-evoked, but not ketamine-evoked, BDNF release from mossy fiber terminals. (**a**) Schematic illustrating viral transduction of CA3 pyramidal neurons with mCherry (red) and BDNF-pH (green), resulting in non-overlapping BDNF-pH-labeled MFT in CA3 (green). (**b, c**) Representative images from acute hippocampal slices from *Grin1*^{flox} mice showing strong mCherry-cre expression (red; deleting GluN1 in CA3 neurons) and non-Cre-dependent BDNF-pH expression (green) in CA3 (**b**), with BDNF-pH-labeled MFTs visualized in CA3 (**c**). (**d, e**) Quantification of BDNF release from MFTs demonstrating that ketamine-evoked secretion (**d**) persists in slices lacking NMDAR function in CA3 neurons, whereas HNK-evoked release (**e**) is abolished. (*p < 0.05, **p* < 0.01, **p < 0.01; one-way ANOVA with Tukey *post hoc* test). Data are mean ± SEM, n = 5-8 animals and 3-11 slices per condition. Scale bars: 30 μm (**b**) and 5 μm (**c**).

Ketamine and HNK rapidly remodel CA3 dendritic spines without altering overall spine density

Reversal of dendritic branch-specific spine loss has been reported following ketamine treatment[25,32], yet the initial drug-evoked effects on structural plasticity within hippocampal CA3 remain unknown. We therefore examined whether rapid alterations in CA3 apical dendritic spines, which receive synaptic input from MFTs, coincide temporally with the acute burst of BDNF release

triggered by ketamine or HNK. Using two-photon microscopy, we imaged eGFP-labeled CA3 apical dendrites in acute slices from Thy1-eGFP mice before and after 30 min of drug exposure (Fig. 5). Based on expression of eGFP in the CA3 region, our analysis was largely contained to second-order distal dendrites extending from the primary branch connected to the soma (Fig. 5a). Ketamine (20 μM) or HNK (10 μM) each drove marked, rapid remodeling of CA3 spines, producing both spine gains and losses across individual dendrites (Fig. 5b-f). Despite these bidirectional effects at the level of single spines, total spine density remained stable, indicating a dynamic redistribution rather than a net change in structural connectivity.

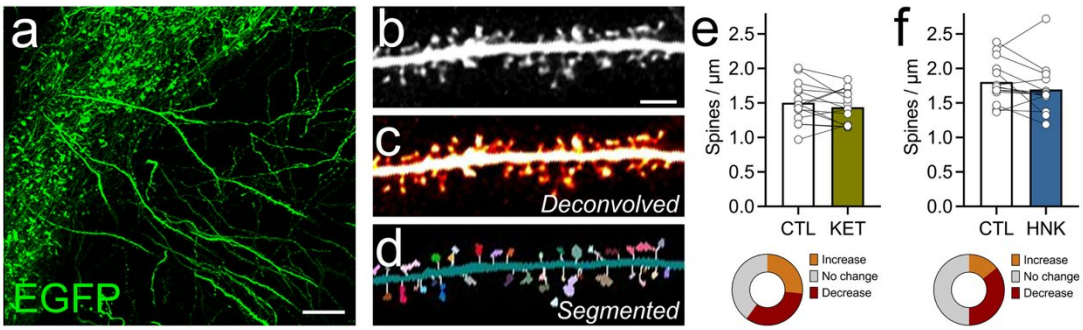

Fig. 5. Ketamine and HNK rapidly remodel CA3 dendritic spines without altering overall spine density. (**a**) Representative image of hippocampal slice from Thy1-eGFP showing dendritic arbors and spines. (**b-d**) Image analysis pipeline illustrating a dendritic segment before processing (**b**), after deconvolution (**c)**, and following automated segmentation (**d**). (**e, f**) Quantification of CA3 spine dynamics demonstrating that 30 min treatment with ketamine (**e**) or HNK (**f**) does not alter overall spine density but induces rapid remodeling of individual spines as shown in the analysis of change in the circle graph below. Both drugs produced proportions of spines that increased in number (26.7 % ketamine; 14.3 % HNK), decreased in number (33.3% ketamine; 35.7% HNK) or remained unchanged (40% ketamine; 50% HNK). Data are mean ± SEM, n = 5-8 animals, 14-15 slices, and 826-926 spines per condition. Scale bars = 30 μm (**a**) and 5 μm (**b-d**).

Discussion

BDNF-dependent synaptic plasticity is essential for the onset of antidepressant actions, yet direct release of BDNF by antidepressant compounds has not been demonstrated. Here we show that ketamine and its metabolite HNK trigger rapid, selective BDNF release from presynaptic mossy fiber terminals within minutes of application. These terminals are enriched in presynaptic NMDARs, which we identify as necessary for BDNF release by both drugs, while postsynaptic NMDARs on CA3 neurons are specifically required for HNK-, but not ketamine-induced, BDNF

release. In parallel, ketamine and HNK each drive fast, bidirectional structural plasticity in CA3 dendritic spines, without altering overall spine density. This dynamic redistribution of hippocampal spine structure, coupled with drug-evoked BDNF release from MFTs, reveals a previously unrecognized synaptic mechanism engaged at the onset of fast-acting antidepressant action.

Numerous studies have linked antidepressant efficacy to increases in hippocampal BDNF levels with subregion specificity[41, 62]. Selective loss of BDNF in the DG, but not CA1, abolishes behavioral responses to classical antidepressants[41], and deletion of its receptor, tropomyosin receptor kinase B (TrkB), in the DG blocks antidepressant-induced neurogenesis[62]. For fast-acting agents such as ketamine, a single infusion into the medial prefrontal cortex or hippocampal DG and CA3 is sufficient to elicit antidepressant-like effects[63, 64]. Within the DG, specific cellular substrates have been identified: activity of immature granule neurons is required for the rapid behavioral response to ketamine, whereas adult neurogenesis supports its sustained effects[65, 66]. Although the DG-dependent role of BDNF in ketamine action has been well described, direct evidence of BDNF release triggered by ketamine or its metabolite HNK has been lacking. Here we show that both compounds acutely evoke BDNF exocytosis from MFTs of DG granule neurons, providing a synapse-specific mechanism that aligns with prior observations of region- and cell type-specific antidepressant actions. These findings suggest that within the first hour of ketamine or HNK exposure, BDNF release in CA3 constitutes a critical early step in initiating the neuropharmacological effects.

Ketamine is a noncompetitive NMDA antagonist, and modulation of NMDAR activity regulates BDNF levels through various cell type-specific mechanisms. In the PFC, tonic inhibition of NMDARs on GABAergic interneurons leads to disinhibition of pyramidal neurons, increasing dendritic spine calcium and promoting BDNF release via mTOR signaling[13, 67]. In the hippocampus, attenuation of resting NMDARs on CA1 glutamatergic neurons by ketamine or HNK enhances local BDNF translation through eukaryotic elongation factor 2 (eEF2) kinase-dependent pathways, thereby increasing synaptic drive and homeostatic plasticity[7, 68, 69]. More recently, typical and fast-acting antidepressants have been shown to directly bind TrkB[70], facilitating BDNF signaling independent of NMDAR blockade. These findings highlight that multiple distinct forms of plasticity[67, 68] and cell-type specific NMDAR mechanisms contribute to acute and sustained phases of antidepressant action. BDNF secretion occurs at both presynaptic and postsynaptic sites [20, 39], and our results reveal an additional layer of synaptic specificity for ketamine and HNK. Presynaptic NMDARs on MFTs were required for the rapid, direct release of BDNF by both drugs,

whereas postsynaptic NMDARs on CA3 dendrites were necessary only for HNK-evoked BDNF release. As MFTs synapse onto both CA3 pyramidal neurons and interneurons, we cannot exclude the contribution of NMDARs on local interneurons, a possibility beyond the scope of the present study. Mossy fiber-CA3 synapses support diverse forms of short-term[71, 72, 73], long-term[72, 74, 75], and homeostatic plasticity[76, 77]. These results place preNMDARs at MFTs as key regulators of ketamine- and HNK-evoked BDNF secretion within the CA3 circuit.

BDNF exocytosis was confined to MFTs and was not detected from dendritic spines within 1 hr of ketamine or HNK treatment. This contrasts with prior work showing that ketamine rapidly increases postsynaptic BDNF translation via eEF2K-eEF2 signaling in hippocampal dendrites[7, 78]. Similarly, we did not observe increases in BDNF release with MK-801, an NMDA antagonist that produces acute antidepressant-like behavioral responses[7, 79], consistent with earlier reports[7, 80]. One possible explanation is that NMDARs containing GluN1/GluN3A subunits and enriched in MFTs, are largely insensitive to open-channel NMDA receptor blockers such as Mg^{2+}, memantine, or MK-801[81, 82]. More broadly, these discrepancies may reflect differences in experimental preparations, brain subregion specificity[83], or methodological differences in quantifying BDNF, as pHluorin-based reporters measure secretion events rather than total protein levels and may not linearly correlate with expression. Our finding that BDNF release originates from MFTs aligns with evidence that both BDNF transcription and translation occur in granule neurons[84] and that activity drives its accumulation in MFTs[18, 84, 85]. The mechanisms governing compartment-specific localization and secretion of BDNF are unclear[19, 86, 87]. Notably, the requirement for postsynaptic NMDARs in HNK-evoked, but not ketamine-evoked, BDNF release suggests that postsynaptic receptor activation can retrogradely modulate presynaptic secretion, potentially through rapid recruitment of trans-synaptic signaling pathways[88, 89, 90]. These observations raise the possibility that fast-acting NMDA antagonists differentially engage presynaptic *versus* postsynaptic release mechanisms depending on synapse type and temporal window of drug action.

In mossy fiber terminals, evoked and spontaneous neurotransmitter release are differentially regulated by glutamate binding to preNMDARs. Activity-dependent release requires Ca^{2+} influx through the receptor, whereas spontaneous transmission can occur via metabotropic NMDAR signaling, independent of ion flux, through conformational changes that engage either Rab3 interacting molecule 1 (RIM1) or c-Jun N-terminal kinase 2 (JNK2) pathways[50]. At resting membrane potentials, the NMDAR pore is largely blocked by extracellular magnesium (Mg^{2+})[91]; however, this block is incomplete under physiological conditions, permitting small residual

currents [92, 93] that can be inhibited by ketamine or MK-801[94 95] through mechanisms involving transient Mg^{2+} block[69, 94] or interactions at distinct binding sites[93]. Our observation that ketamine elicits BDNF release from MFTs aligns with reports that ketamine suppresses spontaneous NMDAR activity at rest[69]. Notably, when residual NMDAR currents were first blocked with MK-801, subsequent treatment with ketamine still triggered robust BDNF release, whereas occluding glutamate binding with APV prior to ketamine attenuated this effect. These findings indicate that channel activation, but not ion flux, is required for ketamine-evoked BDNF exocytosis, consistent with a metabotropic function of preNMDARs in rapid, synapse-specific enhancement of BDNF release.

Both NMDARs and AMPARs have been implicated in the antidepressant actions of ketamine[1, 96]. For HNK, in addition to its reported inhibition of NMDARs[69], early and sustained activation of AMPARs, independent of NMDAR inhibition, has been described[1, 60], suggesting distinct channel-gating effects. In our study, ketamine was applied at 1 μM in dissociated cultures, approximating clinically relevant free plasma concentrations[88], and HNK was applied at 10 nM, consistent with previous work[38]. For acute hippocampal slices, ketamine (20 μM) and HNK (10 μM) were used to account for tissue binding, in line with previous slice studies examining rapid synaptic and structural plasticity[69, 97], and these concentrations were empirically confirmed to evoke robust BDNF release. Under these conditions, both presynaptic and postsynaptic NMDARs were required for HNK-evoked BDNF release.

NMDARs containing GluN3A subunits have unique biophysical, synaptic signaling, and subcellular localization properties compared to canonical tetrameric NMDARs composed of GluN1 and GluN2(A-D) subunits[58]. These receptors display reduced single-channel conductance[98], lower calcium permeability, and diminished sensitivity to Mg^{2+} block at hyperpolarized membrane potentials[99], features that support tonic activation under resting conditions. Consistent with this profile, we confirm GluN3A expression in MFTs and extend prior work demonstrating that preNMDARs facilitate BDNF release at mossy fiber synapses[16]. The presence of GluN3A-containing NMDARs at MFTs provides a mechanistic basis for the sensitivity of presynaptic BDNF release to ketamine and HNK. GluN3A has been shown to assemble with GluN2A or GluN2B subunits in neurons[100, 101], both of which have been implicated in ketamine's cell-type-specific actions in excitatory and inhibitory circuits[59, 67, 102]. Notably, although GluN2B-selective antagonists exhibit antidepressant-like effects in preclinical models[27, 43, 102], these findings have not translated to clinical efficacy[1], underscoring the need to better define subunit-

specific mechanisms. Whether GluN3A-containing NMDARs at MFTs preferentially assemble with GluN2A or GluN2B, and how such assemblies influence ketamine or HNK sensitivity, remains unknown. To our knowledge, this is the first study to implicate GluN3A-containing NMDARs at MFTs as a molecular substrate and a potential therapeutic target in the actions of fast-acting antidepressants. This observation aligns with prior evidence linking GluN3A signaling to enhanced presynaptic release probability, long-term potentiation[103], and improved cognitive performance[104].

Overall spine density in CA3 was unchanged after 30 minutes of ketamine or HNK; however, individual dendritic branches exhibited clear increases or decreases in spine number, indicating that acute structural remodeling was spatially selective rather than global[25]. Although loss of CA3 dendritic spines with ketamine and HNK treatment was unexpected, prior work has shown that ketamine induces loss of distal apical dendritic branches in other circuits, leading to a redistribution of synaptic inputs rather than a net loss of connectivity[31]. Consistent with this framework, spines on hippocampal dendrites are functionally grouped[105, 106, 107], and the likelihood that a spine is gained, lost, or maintained with fast-acting antidepressants may depend on local synaptic inputs and molecular composition. Spines receiving strong glutamatergic or neurotrophic drive, including those enriched for BDNF- or glutamate-sensitive signaling pathways, may be preferentially stabilized or expanded, whereas less active, labile, or silent spines may be selectively pruned.

Future studies will dissect how ketamine and HNK engage distinct presynaptic and postsynaptic mechanisms to regulate mossy fiber-CA3 signaling and structural plasticity. First, targeted manipulation of NMDARs and AMPARs in CA3 pyramidal neurons and local interneurons, using electrophysiology, glycine-site antagonists such as 7-chlorokynurenic acid (7-CKA), and conditional knockouts, will be essential to directly assess receptor activation/inhibition and to determine how metabotropic versus ionotropic NMDAR signaling shapes BDNF release. Parallel *in vivo* work will evaluate whether these synaptic mechanisms translate into antidepressant-like behavioral outcomes. At the molecular level, experiments in *Grin3a*-null mice[103] and with GluN3-selective antagonists[108, 109] will define the specific contribution of GluN3A-containing NMDAR assemblies to ketamine- and HNK-evoked BDNF exocytosis. Finally, integrating analyses of spine subclass and dendritic branch-order, key determinants of synaptic strength, stability, and plasticity[110, 111], with targeted manipulations of BDNF and glutamate signaling[34, 111], will elucidate

how activity at MFTs drives spatially selective spine remodeling, thereby linking subcellular structural plasticity to circuit function and the behavioral efficacy of fast-acting antidepressants.

Materials and Methods

Animals

Sprague Dawley rats were obtained from Charles River Laboratories (Wilmington, MA, USA). Homozygous mouse lines were acquired from Jackson Laboratory (Bar Harbor, ME; Tg(Thy1-EGFP)MJrs/J-#007788, B6.129S4-Grin1^{tm2Stl}/J-#005246, and C57BL/6J-#000664) and bred in-house to maintain colonies. All animals were group-housed under a 12h light/dark cycle with free access to food and water. All animal procedures conformed to the National Institutes of Health *Guide for the Care and Use of Laboratory Animals* and were approved by the Weill Cornell Medicine Institutional Animal Care and Use Committee (IACUC). Animal handling and reporting adhered to ARRIVE guidelines.

Viruses and cDNA constructs

AAV vectors were obtained from UNC Vector Core (University of North Carolina at Chapel Hill, Chapel Hill, NC), including AAV5-CaMKII-mCherry, AAV5-CaMKII-mCherry-cre, control AAV-CaMKIIa-GFP, and AAV-CaMKIIa-GFP-Cre. Additional viral vectors (AAV-hSyn-BDNF-pHluorin, cre-dependent AAV-DJ-DIO-BDNF-pHluorin) were custom-produced by the UNC vector core using plasmids generously provided by Dr. Hyungju park (Korea Brain Research Institute, Daegu, Korea) from UNC Vector Core (AAV-hSyn-BDNF-pHluorin, cre-dependent AAV-DJ-DIO-BDNF-pHluorin). The BDNF-SEP plasmid was obtained from Addgene (#83955; Watertown, MA).

Materials

Ketamine, hydroxynorketamine, and all other chemicals were obtained from Sigma-Aldrich (St.Louis, MO). Isoflurane was purchased from Henry Schein Medical (Melville, NY). All additional reagents were sourced as indicated.

Antibodies

An affinity-purified polyclonal guinea pig anti-Zn_3T antibody, previously characterized[112], was purchased from Synaptic Systems (Goettingen, Germany). A polyclonal rabbit anti-GluN3A antibody (recognizing amino acids 1098-1113 of rat GluN3A), previously validated in [48], was also used.

GluN3A Immuno-electron microscopy

Electron microscopic immunolocalization of GluN3A was performed using the pre-embedding silver intensified immunogold method as described previously[113]. Briefly, mice were deeply anesthetized with pentobarbital (150mg/kg; i.p.) and perfused through the aorta sequentially with: 1) ~5 ml 0.9% NaCl containing 1,000 units/ml heparin; and 2) 30 ml 3.75% acrolein and 2% paraformaldehyde in 0.1 M phosphate buffer (PB; pH 7.4). The brain was post-fixed in in 2% acrolein and 2% paraformaldehyde in PB for 30 min. and then the region containing the hippocampal formation (HF) was cut into a 5-mm-thick coronal block using a brain mold. Sections (40 μm thick) were cut through the HF on a vibrating microtome (VT1000 Leica Microsystems) and the sections were stored in 24 well plates in cryoprotectant solution (30% sucrose, 30% ethylene glycol in PB) at −20°C until use. Two dorsal hippocampal sections per mouse were selected from each experimental condition and coded by hole-punches in the cortex. The sections were then placed in a single container and processed together through all immunocytochemical procedures to ensure identical labeling conditions. Sections were incubated in 1% sodium borohydride in PB for 30 min to neutralize reactive aldehydes then rinsed in PB ~10 times until gaseous bubbling ceased.

Sections were rinsed in 0.1 M Tris saline (TS; pH 7.6) followed by an incubation in 0.5% BSA in TS for 30 min to reduce nonspecific labeling. Sections then were incubated in rabbit anti-GluN3A (1:50) in 0.1% BSA in TS for 1 day at RT and then 1 day at 4°C. Sections were rinsed in TS followed by washing buffer [0.1 M phosphate-buffered saline (PBS) with 2% gelatin and 0.1% BSA], and incubated overnight at 4°C in a 1:50 dilution of donkey anti-rabbit IgG conjugated to 1-nm gold particles [Electron Microscopy Sciences (EMS) Cat# 810.311] in 0.01% gelatin and 0.08% BSA. All primary and secondary antibody incubations were carried out at 145 rpm, and all rinses were conducted at 90 rpm on a rotator shaker. Sections were rinsed in PBS, post-fixed in 2% glutaraldehyde in PBS for 10 min, then rinsed in PBS and in 0.2 M sodium citrate buffer (pH 7.4). The conjugated gold particles were enhanced using silver solution silver solution (SEKL15 Silver enhancement kit, Prod No. 15718 Ted Pella Inc.) for 9 min. Sections were fixed in 2% osmium tetroxide for 1 h, dehydrated in increasing ethanol concentrations to propylene oxide and embedded in EMBed 812 (EMS) between two sheets of Aclar plastic (Honeywell, Pottsville, PA). Ultrathin sections (70 nm) of the CA3 were cut with a Diatome diamond knife (EMS) on a Leica UCT6 ultratome and were collected on 400 mesh thin-bar copper grids (T400-Cu, EMS). The grids were counterstained with Uranylless™ (catalog #22409, EMS) and lead citrate (catalog #22410 EMS). Specimens were imaged on a Hitachi HT7800 transmission electron microscope.

Hippocampal neuron culture and transfection

Primary rat hippocampal neurons were cultured as described previously[114]. Briefly, hippocampi were dissected from embryonic day 16–18 (E16–18) Sprague Dawley rat embryos, dissociated using papain, and plated on Lab-Tek II chambered borosilicate coverglass (4.0 cm²/well; NUNC, Rochester, NY) at a density of 200,000 cells/mm². Cells were maintained in Neurobasal medium (GIBCO, Grand Island, NY) supplemented with SM1 (Stem Cell Technologies, Vancouver, BC, Canada) and 0.5 mM L-glutamine (Sigma-Aldrich, St. Louis, MO). At 16 days *in vitro* (DIV), cultures were co-transfected using calcium phosphate precipitation with 6–10 µg of total DNA containing of a CAG-driven mCherry plasmid and BDNF-SEP to visualize neuronal morphology and BDNF release, respectively. Cells were incubated with the transfection mixture for 2.5–3 hours at 37°C (95% air and 5% CO_2), rinsed twice with pre-warmed HEPES-buffered solution (HBS; in mM: 135 NaCl, 4 KCl, 1 Na_2HPO_4, 2 $CaCl_2$, 1 $MgCl_2$, 10 glucose, and 20 HEPES; pH 7.35), and returned to fresh Neurobasal medium. Neurons were used for live-cell imaging at 21 DIV.

Stereotaxic surgery

Adult *Grin1*^{flox} and wild-type mice (P23-35; males and females) were anesthetized with isoflurane (3% vol induction; 1.5% vol maintenance) and secured in a stereotaxic frame (Kopf Instruments, Tujunga, CA). For knockdown of *GRIN1* and expression of BDNF in DG granule neurons, a mixture of AAV5-CamKII-mCherry-cre and cre-dependent AAV-DJ-DIO-BDNF-pHluorin was injected into the DG of the hippocampus (mediolateral, 1.5 mm; anteroposterior, -2.18 mm; dorsoventral, 2.2mm from bregma)[115] at a rate of 0.1 µL/min. A total volume of 1 µL (1:2 ratio) was delivered unilaterally, and the needle remained in place for at least 10 min post-injection. For knockdown of *GRIN1* and expression of BDNF in CA3 pyramidal neurons, a mixture of AAV5-CamKII-mCherry-cre and AAV-hSyn-BDNF-pHluorin was injected into the CA3 (mediolateral, 1.8 mm; anteroposterior, -1.9 mm; dorsoventral, 2.2mm from bregma)[115] at a rate of 50 nL/min. A total volume of 500 nL (1:2 ratio) was injected unilaterally and the needle left in place for at least 10 min after the injection. Following surgery, mice were monitored for 1 h, returned to their home cages, and allowed to recover for 2-4 weeks before experimentation.

Acute hippocampal slice preparation

Acute hippocampal slices were prepared with modifications as previously described[16]. Two-to-four weeks post-surgery, mice were anesthetized with isoflurane and decapitated. The

hippocampus was rapidly dissected, and 300 μm-thick slices were cut using a VT1200S vibratome (Leica Microsystems, Deerfield, IL) in ice-cold NMDG solution containing (in mM): 93 NMDG, 2.5 KCl, 1.25 NaH_2PO_4, 30 $NaHCO_3$, 20 HEPES, 25 glucose, 5 sodium ascorbate, 2 thiourea, 3 sodium pyruvate, 10 $MgCl_2$, and 0.5 $CaCl_2$. Slices were transferred to a recovery chamber maintained at 32–34°C and incubated for 30 min in oxygenated artificial cerebrospinal fluid (ACSF) containing (in mM): 124 NaCl, 2.5 KCl, 26 $NaHCO_3$, 1 NaH_2PO_4, 2.5 $CaCl_2$, 1.3 $MgSO_4$, and 10 D-glucose. All solutions were continuously bubbled with 95% O_2 and 5% CO_2 (pH 7.4). After recovery, slices were maintained at room temperature until imaging experiments.

Confocal time-lapse imaging

Neuronal cultures were transferred to a temperature- and humidity-controlled imaging chamber and equilibrated in a modified Tyrode's solution containing (in mM): 119 NaCl, 2.5 KCl, 2 $CaCl_2$, 2 $MgCl_2$, 25 HEPES, and 30 glucose (pH 7.4). Time-lapse recordings were performed using a 63x/1.4NA Plan-APO oil-immersion objective (Zeiss, Thornwood, NY) on a Zeiss Axio Observer Z1 microscope equipped with a CSU-X spinning-disk confocal scanner (Yokogawa, Wayne, PA). Samples were excited with a laser launch equipped with 50mW solid-state lasers (488 nm, 561 nm), and fluorescence emission was collected through 525/50 or 629/62 band-pass filters. Images were acquired at 1 min intervals for 60 min using an Orca Flash4 camera (Hamamatsu, Bridgewater, NJ) and Zeiss Zen Blue software. Z-stacks were acquired at of 0.2 to 0.4 μm optical section thickness. BDNF-SEP fluorescence responses were measured in the following order: 3 min baseline recording, 57 min Tyrode's solution alone or Tyrode's solution with ketamine (1 μM) or HNK (10 nM), followed by NH_4Cl alkalization. For pharmacological experiments with NMDA channel blockers, neurons were preincubated with Tyrode's solution containing AP5 (50 μM) or MK801 (10 μM) for 3 min prior to ketamine application.

Two-Photon Imaging

Two to four weeks post-surgery, acute hippocampal slices were prepared as described, and slices showing optimal GFP and mCherry expression were selected for imaging. Fluorescence changes were acquired using a Prairie Investigator two-photon microscopy system equipped with a resonant galvo scanning module (Bruker, Billerica, MA). A Chameleon Discovery TPC laser (Coherent, Saxonburg, PA) tuned to 920nm was used for excitation and signals were collected through GaAsP photomultiplier tubes (Hamamatsu, Bridgewater, NJ) with a 20x/1.0NA objective (Olympus, Tokyo, Japan) at 6.4x zoom. Imaging sites were identified by the presence of axons and large mossy fiber boutons (≥3 μm) in the *stratum lucidum* and captured at 512 x 512 pixel

resolution. For presynaptic *GRIN1* knockdown (DG viral injections), mossy fiber terminals co-expressing Cre-dependent BDNF-pHluorin (green) and Cre-dependent mCherry (red) were selected as regions of interest (ROIs). For postsynaptic *GRIN1* knockdown (CA3 viral injections), terminals expressing only non-Cre dependent BDNF-pHluorin were chosen. Boutons expressing Cre-dependent mCherry alone were excluded to avoid retrograde viral spread and unintended *GRIN1* deletion in granule neurons. The time course measurements of BDNF-pH fluorescence were collected under the following sequence: a 1 min ACSF baseline, followed by 5 min of ACSF alone or ACSF containing ketamine (20 μM) or HNK (10 μM). Images were acquired at 1 Hz using T-series software (PrairieView 5.4, Bruker), as modified from[16, 116].

For imaging CA3 dendritic spines, acute slices from Thy1-eGFP mice were scanned using the same system, with the addition of a piezoelectric z-axis controller and a 40×/0.8 NA objective (Nikon, Tokyo, Japan). Imaging sties were identified by dendritic morphology in the *stratum lucidum* or *stratum radiatum*. Spines, primarily located on second-order apical dendrites, were selected as ROIs from 512 × 512-pixel images (78 × 78 μm field of view; pixel size: 0.152 μm; *z*-step: 0.5 μm). Two Z-stacks were collected for each slice: one immediately after initiating ACSF perfusion (baseline) and after 30 minutes of continuous perfusion with ACSF alone, ACSF + ketamine (20 μM), or ACSF + HNK (10 μM).

Image and statistical analysis

Electron microscopy: All analyses were done by persons who were blind to experimental groups. Ultrathin sections from 3 mice in each experimental condition was analyzed at the tissue-plastic interface to minimize the difference in antibody penetration[55]. Immunolabeled profiles were classified using defined morphological criteria[117]. Dendritic profiles contain cytoplasm with mitochondria, microtubules, and agranular reticulum and were postsynaptic to axon terminal profiles identified by the presence of vesicles. Mossy fiber pathway terminals are identified by their large size (1-2 μm in diameter) and often contact multiple dendritic spines of the CA3 pyramidal cell dendrites[118]. For quantification, 50 GluN3A-labeled mossy fiber terminals from randomly selected 3,555 nm^2 fields in CA3 were analyzed, and GluN3A-immunogold particles were manually counted within mossy terminals and their postsynaptic spines.

BDNF-SEP: Asynchronous BDNF release from neuronal cultures is well documented and was quantified as the number of events, rather than changes in fluorescence intensity[114, 119]. All images were background-subtracted, corrected for XY drift using the StackReg plugin in ImageJ, and sequential frames were aligned to ensure accurate tracking of BDNF release events and to

prevent motion artifacts from influencing fluorescence measurements. ROIs were selected based on mCherry-labeled (red) boutons to restrict analysis to BDNF release events originating from mossy fiber terminals. Detection of fluorescence changes indicating BDNF release within each ROI was performed using a custom-modified graphical user interface (MATLAB; Fluorosnnap; University of Pennsylvania) which automatically determined fluorescence thresholds, filtered particle size, and excluded events outside the defined ROI. Fluorescence intensity for each detected event was calculated by measuring the change from baseline fluorescence using a custom Time Series Analyzer plugin in ImageJ. Each event underwent signal-to-noise ratio (SNR) analysis, and ΔF was defined as the difference peak fluorescence (F_{peak}) and baseline fluorescence ($F_{baseline}$). Release events counted only if mean ΔF was>5 SD above the baseline mean. Baseline fluorescence ($F_{baseline}$) was calculated from three frames acquired over a 3-min period prior to treatment. and ΔF was calculated as the difference between the peak fluorescence (F_{peak}) and $F_{baseline}$. Because each FOV contained a different number of boutons, event frequency was normalized by dividing total number of BDNF release events by the number of boutons within that FOV. Each imaging session ended with alkalization using 50 mM NH_4Cl to confirm localization of BDNF-pH and to verify cell responsiveness. BDNF trafficking particles were excluded from the analysis, and only NH_4Cl-responsive cells were included.

BDNF-pHluorin: All images were background-subtracted, corrected for XY drift during acquisition using the Movie Aligner plugin in ImageJ (NIH, Bethesda, MD), and aligned frame-by-frame previously as described[120] to ensure accurate tracking of BDNF release events and prevent motion artifacts from influencing fluorescence measurements. ROIs were identified manually, and fluorescence intensity was quantified for each ROI relative to its baseline. The difference between F_{peak} and $F_{baseline}$ was used to calculate ΔF, and values were reported as ΔF/F of the BDNF-pHluorin signal[16] using ImageJ (Time series analyzer, NIH).

Quantitative spine analysis: Dendritic branches from acquired images were processed using Huygens deconvolution software (Scientific Volume Imaging, Hilversum, Netherlands) to enhance SNR ratio and spatial resolution. Following deconvolution, spine density was quantified using Restoration Enhanced Spine and Neuron Analysis (RESPAN) by selecting dendritic segments or ROIs of fixed length and width for each neuron, with each ROI containing at least 45 spines[121, 122]. Dendritic arbors were segmented to identify spine heads and necks from eGFP fluorescence using an adaptive, self-configuring nnU-Net architecture[123]. Subsequent processing in RESPAN, using the Model 3 pre-trained segmentation model available through the official GitHub repository,

generated three-dimensional spine detection outputs that were used to quantify spine density, reported as spines per micrometer of dendrite. To minimize false positives, spines were retained only if their volumes ranged from 0.03 to 15 μm^3 and their distances from the parent dendrite were below the defined threshold. Dendrite segments with total volumes < 3 μm^3 were excluded. Individual spine numbers were measured at baseline (0 min) and after 30 min, normalized to baseline values, and classified as increased (>10%), decreased (<10%), or unchanged. Across experimental groups, 375 - 925 spines were analyzed grouper condition. Automated spine detection and density measurements were independently validated by manual spine counts conducted on both original and deconvolved images.

Data analysis

All analyses were performed with the experimenter blinded to experimental conditions. Statistical comparisons were conducted using unpaired two-tailed Student *t*-tests or ordinary one-way ANOVA, followed by Tukey *post-hoc* tests, as appropriate, using GraphPad Prism v10 (Graphpad Software, Inc., San Diego, CA). A significance threshold of $p < 0.05$ was applied. Data are presented as mean ± SEM unless otherwise indicated. Asterisks denote values significantly different from control (Ctl): $^{*}p < 0.05$, $^{**}p < 0.01$, $^{***}p < 0.001$, $^{****}p < 0.0001$.

Acknowledgments

We thank Dr. Hyungju Park (Korea Brain Research Institute, Daegu, Korea) for generously providing plasmids for viral vectors of BDNF-pH. We thank Mark Koenis (Huygens; Scientific Volume Imaging, Hilversum, Netherlands) and Luke Hammond (RESPAN) for their help with data processing for spine quantification. We also thank Ms. June Chan of the Neuroanatomy EM core, Feil Family Brain and Mind Research Institute for technical assistance.

Author contributions:

JP, ILAR, and HCH contributed to study conception and design. Material preparation, data collection, and analysis were performed by ILAR for figures 1,2 (panels e and f) 3,4, and 5 and by KP, HA, and SZ for figure 2 (panels a-d). Custom macros were written by KWJ. Figures were prepared by ILAR, KH, and JP. The original draft of the manuscript was written by JP, with additional review and editing by JP, HCH, and TAM. All authors approved the final manuscript.

Funding

US National Institutes of Health grant R01 GM130722 to JP and GM58055 to HCH. The Hitachi HT7800 Transmission electron microscope was obtained by the NIH shared instrument grant (1S10OD026974-01A1).

Supplementary Information for

Presynaptic NMDA receptors at mossy fiber terminals mediate rapid BDNF release by ketamine and hydroxynorketamine

Irem L. Atasoy-Rodriguez[1], Kenneth W. Johnson[2], Kishan Patel[1], Haroon Arain[3], Syed Zaidi[3], Karl F. Herold[1], Teresa A. Milner[3], Hugh C. Hemmings Jr.[1,2], Jimcy Platholi[1,3#]

[1]Department of Anesthesiology, Weill Cornell Medicine, New York, NY, USA
[2]Department of Pharmacology, Weill Cornell Medicine, New York, NY, USA
[3]Feil Family Brain and Mind Research Institute, Weill Cornell Medicine, New York, NY, USA

[#]Corresponding author: jip2003@med.cornell.edu

Supplementary Video 1 (attached): Ketamine (1 μM) evokes rapid release of BDNF

Supplementary Figures 1 and 2

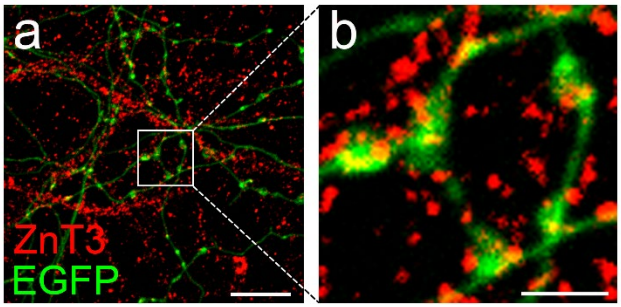

Fig. S1: Zinc transporter 3 (ZnT3) is expressed in mossy fiber terminals. Immunofluorescence images showing axons (**a**) with close-up of mossy fiber terminals (**b**) labeled with ZnT3. Scale bars = 10 μm (**a**) and 5 μm (**b**).

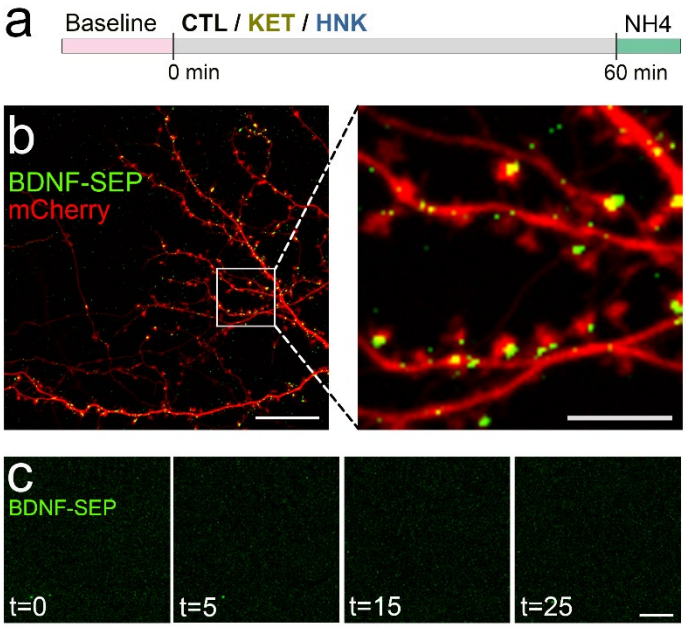

Fig. S2. Ketamine or HNK does not release BDNF from hippocampal dendritic spines. Rat hippocampal neuron cultures (21 DIV) transfected with BDNF-SEP and mCherry were perfused with 1μM ketamine, 10nM HNK, or control buffer and imaged as indicated in (**a**). Representative images showing dendritic arbor of a control neuron (**b,** left) with close-up of dendritic spines (**b**, right) after alkalinization with BDNF-SEP pools in spines. Representative images showing single BDNF exocytotic events before (**c**, t=0) and after (**b**, t=5-25) ketamine application with no release of BDNF detected. Scale bar = 10 μm (**b,** left; **c**) and 5 μm (**b,** right).

References

1. Zanos P, Gould TD. Mechanisms of ketamine action as an antidepressant. *Mol Psychiatry* **23**, 801-811 (2018).

2. Nierenberg AA*, et al.* Timing of onset of antidepressant response with fluoxetine treatment. *Am J Psychiatry* **157**, 1423-1428 (2000).

3. Berman RM*, et al.* Antidepressant effects of ketamine in depressed patients. *Biol Psychiatry* **47**, 351-354 (2000).

4. Kishimoto T*, et al.* Single-dose infusion ketamine and non-ketamine N-methyl-d-aspartate receptor antagonists for unipolar and bipolar depression: a meta-analysis of efficacy, safety and time trajectories. *Psychol Med* **46**, 1459-1472 (2016).

5. Muller J, Pentyala S, Dilger J, Pentyala S. Ketamine enantiomers in the rapid and sustained antidepressant effects. *Ther Adv Psychopharmacol* **6**, 185-192 (2016).

6. Park M, Niciu MJ, Zarate CA, Jr. Novel Glutamatergic Treatments for Severe Mood Disorders. *Curr Behav Neurosci Rep* **2**, 198-208 (2015).

7. Autry AE*, et al.* NMDA receptor blockade at rest triggers rapid behavioural antidepressant responses. *Nature* **475**, 91-95 (2011).

8. Duman RS, Monteggia LM. A neurotrophic model for stress-related mood disorders. *Biol Psychiatry* **59**, 1116-1127 (2006).

9. Cowansage KK, LeDoux JE, Monfils MH. Brain-derived neurotrophic factor: a dynamic gatekeeper of neural plasticity. *Curr Mol Pharmacol* **3**, 12-29 (2010).

10. Pittenger C, Duman RS. Stress, depression, and neuroplasticity: a convergence of mechanisms. *Neuropsychopharmacology* **33**, 88-109 (2008).

11. Fraga DB*, et al.* Ketamine alters behavior and decreases BDNF levels in the rat brain as a function of time after drug administration. *Braz J Psychiatry* **35**, 262-266 (2013).

12. Lepack AE, Fuchikami M, Dwyer JM, Banasr M, Duman RS. BDNF release is required for the behavioral actions of ketamine. *Int J Neuropsychopharmacol* **18**, (2014).

13. Lepack AE, Bang E, Lee B, Dwyer JM, Duman RS. Fast-acting antidepressants rapidly stimulate ERK signaling and BDNF release in primary neuronal cultures. *Neuropharmacology* **111**, 242-252 (2016).

14. Ma Z*, et al.* TrkB dependent adult hippocampal progenitor differentiation mediates sustained ketamine antidepressant response. *Nat Commun* **8**, 1668 (2017).

15. Schmidt HD, Shelton RC, Duman RS. Functional biomarkers of depression: diagnosis, treatment, and pathophysiology. *Neuropsychopharmacology* **36**, 2375-2394 (2011).

16. Lituma PJ, Kwon HB, Alviña K, Luján R, Castillo PE. Presynaptic NMDA receptors facilitate short-term plasticity and BDNF release at hippocampal mossy fiber synapses. *Elife* **10**, (2021).

17. Buzsáki G. Feed-forward inhibition in the hippocampal formation. *Prog Neurobiol* **22**, 131-153 (1984).

18. Danzer SC, McNamara JO. Localization of brain-derived neurotrophic factor to distinct terminals of mossy fiber axons implies regulation of both excitation and feedforward inhibition of CA3 pyramidal cells. *J Neurosci* **24**, 11346-11355 (2004).

19. Sasi M, Vignoli B, Canossa M, Blum R. Neurobiology of local and intercellular BDNF signaling. *Pflugers Arch* **469**, 593-610 (2017).

20. Dieni S*, et al.* BDNF and its pro-peptide are stored in presynaptic dense core vesicles in brain neurons. *J Cell Biol* **196**, 775-788 (2012).

21. Kobayashi K. Targeting the hippocampal mossy fiber synapse for the treatment of psychiatric disorders. *Mol Neurobiol* **39**, 24-36 (2009).

22. Duman RS, Li N. A neurotrophic hypothesis of depression: role of synaptogenesis in the actions of NMDA receptor antagonists. *Philos Trans R Soc Lond B Biol Sci* **367**, 2475-2484 (2012).

23. Kang HJ*, et al.* Decreased expression of synapse-related genes and loss of synapses in major depressive disorder. *Nat Med* **18**, 1413-1417 (2012).

24. Holmes SE*, et al.* Lower synaptic density is associated with depression severity and network alterations. *Nat Commun* **10**, 1529 (2019).

25. Moda-Sava RN*, et al.* Sustained rescue of prefrontal circuit dysfunction by antidepressant-induced spine formation. *Science* **364**, (2019).

26. Wu M, Minkowicz S, Dumrongprechachan V, Hamilton P, Kozorovitskiy Y. Ketamine Rapidly Enhances Glutamate-Evoked Dendritic Spinogenesis in Medial Prefrontal Cortex Through Dopaminergic Mechanisms. *Biol Psychiatry* **89**, 1096-1105 (2021).

27. Li N*, et al.* mTOR-dependent synapse formation underlies the rapid antidepressant effects of NMDA antagonists. *Science* **329**, 959-964 (2010).

28. Pryazhnikov E*, et al.* Longitudinal two-photon imaging in somatosensory cortex of behaving mice reveals dendritic spine formation enhancement by subchronic administration of low-dose ketamine. *Sci Rep* **8**, 6464 (2018).

29. Treccani G*, et al.* S-Ketamine Reverses Hippocampal Dendritic Spine Deficits in Flinders Sensitive Line Rats Within 1 h of Administration. *Mol Neurobiol* **56**, 7368-7379 (2019).

30. Zhang J, Qu Y, Chang L, Pu Y, Hashimoto K. (R)-Ketamine Rapidly Ameliorates the Decreased Spine Density in the Medial Prefrontal Cortex and Hippocampus of Susceptible Mice After Chronic Social Defeat Stress. *Int J Neuropsychopharmacol* **22**, 675-679 (2019).

31. Phoumthipphavong V, Barthas F, Hassett S, Kwan AC. Longitudinal Effects of Ketamine on Dendritic Architecture In Vivo in the Mouse Medial Frontal Cortex. *eNeuro* **3**, (2016).

32. Liao C, Dua AN, Wojtasiewicz C, Liston C, Kwan AC. Structural neural plasticity evoked by rapid-acting antidepressant interventions. *Nat Rev Neurosci*, (2024).

33. Ng LHL, Huang Y, Han L, Chang RC, Chan YS, Lai CSW. Ketamine and selective activation of parvalbumin interneurons inhibit stress-induced dendritic spine elimination. *Transl Psychiatry* **8**, 272 (2018).

34. Harward SC*, et al.* Autocrine BDNF-TrkB signalling within a single dendritic spine. *Nature* **538**, 99-103 (2016).

35. Murakoshi H, Wang H, Yasuda R. Local, persistent activation of Rho GTPases during plasticity of single dendritic spines. *Nature* **472**, 100-104 (2011).

36. Castrén E, Monteggia LM. Brain-Derived Neurotrophic Factor Signaling in Depression and Antidepressant Action. *Biol Psychiatry* **90**, 128-136 (2021).

37. Riggs LM, Pereira EFR, Thompson SM, Gould TD. cAMP-dependent protein kinase signaling is required for (2R,6R)-hydroxynorketamine to potentiate hippocampal glutamatergic transmission. *J Neurophysiol* **131**, 64-74 (2024).

38. Fukumoto K*, et al.* Activity-dependent brain-derived neurotrophic factor signaling is required for the antidepressant actions of (2R,6R)-hydroxynorketamine. *Proc Natl Acad Sci U S A* **116**, 297-302 (2019).

39. Matsuda N*, et al.* Differential activity-dependent secretion of brain-derived neurotrophic factor from axon and dendrite. *J Neurosci* **29**, 14185-14198 (2009).

40. Taliaz D, Stall N, Dar DE, Zangen A. Knockdown of brain-derived neurotrophic factor in specific brain sites precipitates behaviors associated with depression and reduces neurogenesis. *Mol Psychiatry* **15**, 80-92 (2010).

41. Adachi M, Barrot M, Autry AE, Theobald D, Monteggia LM. Selective loss of brain-derived neurotrophic factor in the dentate gyrus attenuates antidepressant efficacy. *Biol Psychiatry* **63**, 642-649 (2008).

42. Abdallah CG, Sanacora G, Duman RS, Krystal JH. Ketamine and rapid-acting antidepressants: a window into a new neurobiology for mood disorder therapeutics. *Annu Rev Med* **66**, 509-523 (2015).

43. Maeng S*, et al.* Cellular mechanisms underlying the antidepressant effects of ketamine: role of alpha-amino-3-hydroxy-5-methylisoxazole-4-propionic acid receptors. *Biol Psychiatry* **63**, 349-352 (2008).

44. Yang C, Hu YM, Zhou ZQ, Zhang GF, Yang JJ. Acute administration of ketamine in rats increases hippocampal BDNF and mTOR levels during forced swimming test. *Ups J Med Sci* **118**, 3-8 (2013).

45. Abbott JA, Popescu GK. Hydroxynorketamine Blocks N-Methyl-d-Aspartate Receptor Currents by Binding to Closed Receptors. *Mol Pharmacol* **98**, 203-210 (2020).

46. Aleksandrova LR, Wang YT, Phillips AG. Hydroxynorketamine: Implications for the NMDA Receptor Hypothesis of Ketamine's Antidepressant Action. *Chronic Stress (Thousand Oaks)* **1**, (2017).

47. Banerjee A, Meredith RM, Rodríguez-Moreno A, Mierau SB, Auberson YP, Paulsen O. Double dissociation of spike timing-dependent potentiation and depression by subunit-preferring NMDA receptor antagonists in mouse barrel cortex. *Cereb Cortex* **19**, 2959-2969 (2009).

48. Larsen RS*, et al.* NR3A-containing NMDARs promote neurotransmitter release and spike timing-dependent plasticity. *Nat Neurosci* **14**, 338-344 (2011).

49. Larsen RS*, et al.* Synapse-specific control of experience-dependent plasticity by presynaptic NMDA receptors. *Neuron* **83**, 879-893 (2014).

50. Wong HH, Rannio S, Jones V, Thomazeau A, Sjöström PJ. NMDA receptors in axons: there's no coincidence. *J Physiol* **599**, 367-387 (2021).

51. Nabavi S, Kessels HW, Alfonso S, Aow J, Fox R, Malinow R. Metabotropic NMDA receptor function is required for NMDA receptor-dependent long-term depression. *Proc Natl Acad Sci U S A* **110**, 4027-4032 (2013).

52. Nabavi S, Fox R, Proulx CD, Lin JY, Tsien RY, Malinow R. Engineering a memory with LTD and LTP. *Nature* **511**, 348-352 (2014).

53. Stein IS, Park DK, Flores JC, Jahncke JN, Zito K. Molecular Mechanisms of Non-ionotropic NMDA Receptor Signaling in Dendritic Spine Shrinkage. *J Neurosci* **40**, 3741-3750 (2020).

54. Dore K, Stein IS, Brock JA, Castillo PE, Zito K, Sjöström PJ. Unconventional NMDA Receptor Signaling. *J Neurosci* **37**, 10800-10807 (2017).

55. Milner TA, Waters, E.M., Robinson, D.C., Pierce, J.P. Degenerating processes identified by electron microscopic immunocytochemical methods. *Neurodegeneration, Methods and Protocols*, 23-59 (2011).

56. Pachernegg S, Strutz-Seebohm N, Hollmann M. GluN3 subunit-containing NMDA receptors: not just one-trick ponies. *Trends Neurosci* **35**, 240-249 (2012).

57. Abrahamsson T*, et al.* Differential Regulation of Evoked and Spontaneous Release by Presynaptic NMDA Receptors. *Neuron* **96**, 839-855.e835 (2017).

58. Crawley O, Conde-Dusman MJ, Pérez-Otaño I. GluN3A NMDA receptor subunits: more enigmatic than ever? *J Physiol* **600**, 261-276 (2022).

59. Su T, Lu Y, Fu C, Geng Y, Chen Y. GluN2A mediates ketamine-induced rapid antidepressant-like responses. *Nat Neurosci* **26**, 1751-1761 (2023).

60. Zanos P*, et al.* NMDAR inhibition-independent antidepressant actions of ketamine metabolites. *Nature* **533**, 481-486 (2016).

61. Piazza MK, Kavalali ET, Monteggia LM. Ketamine induced synaptic plasticity operates independently of long-term potentiation. *Neuropsychopharmacology* **49**, 1758-1766 (2024).

62. Li Y*, et al.* TrkB regulates hippocampal neurogenesis and governs sensitivity to antidepressive treatment. *Neuron* **59**, 399-412 (2008).

63. Shirayama Y, Hashimoto K. Effects of a single bilateral infusion of R-ketamine in the rat brain regions of a learned helplessness model of depression. *Eur Arch Psychiatry Clin Neurosci* **267**, 177-182 (2017).

64. Yang C*, et al.* Mechanistic Target of Rapamycin-Independent Antidepressant Effects of (R)-Ketamine in a Social Defeat Stress Model. *Biol Psychiatry* **83**, 18-28 (2018).

65. Rawat R, Tunc-Ozcan E, McGuire TL, Peng CY, Kessler JA. Ketamine activates adult-born immature granule neurons to rapidly alleviate depression-like behaviors in mice. *Nat Commun* **13**, 2650 (2022).

66. Rawat R*, et al.* Ketamine's rapid and sustained antidepressant effects are driven by distinct mechanisms. *Cell Mol Life Sci* **81**, 105 (2024).

67. Ali F*, et al.* Ketamine disinhibits dendrites and enhances calcium signals in prefrontal dendritic spines. *Nat Commun* **11**, 72 (2020).

68. Kavalali ET, Monteggia LM. Targeting Homeostatic Synaptic Plasticity for Treatment of Mood Disorders. *Neuron* **106**, 715-726 (2020).

69. Suzuki K, Nosyreva E, Hunt KW, Kavalali ET, Monteggia LM. Effects of a ketamine metabolite on synaptic NMDAR function. *Nature* **546**, E1-e3 (2017).

70. Casarotto PC*, et al.* Antidepressant drugs act by directly binding to TRKB neurotrophin receptors. *Cell* **184**, 1299-1313.e1219 (2021).

71. Salin PA, Scanziani M, Malenka RC, Nicoll RA. Distinct short-term plasticity at two excitatory synapses in the hippocampus. *Proc Natl Acad Sci U S A* **93**, 13304-13309 (1996).

72. Nicoll RA, Schmitz D. Synaptic plasticity at hippocampal mossy fibre synapses. *Nat Rev Neurosci* **6**, 863-876 (2005).

73. Vandael D, Borges-Merjane C, Zhang X, Jonas P. Short-Term Plasticity at Hippocampal Mossy Fiber Synapses Is Induced by Natural Activity Patterns and Associated with Vesicle Pool Engram Formation. *Neuron* **107**, 509-521.e507 (2020).

74. Zalutsky RA, Nicoll RA. Comparison of two forms of long-term potentiation in single hippocampal neurons. *Science* **248**, 1619-1624 (1990).

75. Weisskopf MG, Castillo PE, Zalutsky RA, Nicoll RA. Mediation of hippocampal mossy fiber long-term potentiation by cyclic AMP. *Science* **265**, 1878-1882 (1994).

76. Mendez P, Stefanelli T, Flores CE, Muller D, Lüscher C. Homeostatic Plasticity in the Hippocampus Facilitates Memory Extinction. *Cell Rep* **22**, 1451-1461 (2018).

77. Lee KJ*, et al.* Mossy fiber-CA3 synapses mediate homeostatic plasticity in mature hippocampal neurons. *Neuron* **77**, 99-114 (2013).

78. Suzuki K, Monteggia LM. The role of eEF2 kinase in the rapid antidepressant actions of ketamine. *Adv Pharmacol* **89**, 79-99 (2020).

79. Yang BK, Qin J, Nie Y, Chen JC. Sustained antidepressant action of the N-methyl-D-aspartate receptor antagonist MK-801 in a chronic unpredictable mild stress model. *Exp Ther Med* **16**, 5376-5383 (2018).

80. Trullas R, Skolnick P. Functional antagonists at the NMDA receptor complex exhibit antidepressant actions. *Eur J Pharmacol* **185**, 1-10 (1990).

81. Chatterton JE*, et al.* Excitatory glycine receptors containing the NR3 family of NMDA receptor subunits. *Nature* **415**, 793-798 (2002).

82. Madry C, Mesic I, Bartholomäus I, Nicke A, Betz H, Laube B. Principal role of NR3 subunits in NR1/NR3 excitatory glycine receptor function. *Biochem Biophys Res Commun* **354**, 102-108 (2007).

83. Castrén E, da Penha Berzaghi M, Lindholm D, Thoenen H. Differential effects of MK-801 on brain-derived neurotrophic factor mRNA levels in different regions of the rat brain. *Exp Neurol* **122**, 244-252 (1993).

84. Smith MA, Zhang LX, Lyons WE, Mamounas LA. Anterograde transport of endogenous brain-derived neurotrophic factor in hippocampal mossy fibers. *Neuroreport* **8**, 1829-1834 (1997).

85. Wetmore C, Olson L, Bean AJ. Regulation of brain-derived neurotrophic factor (BDNF) expression and release from hippocampal neurons is mediated by non-NMDA type glutamate receptors. *J Neurosci* **14**, 1688-1700 (1994).

86. Wang CS, Kavalali ET, Monteggia LM. BDNF signaling in context: From synaptic regulation to psychiatric disorders. *Cell* **185**, 62-76 (2022).

87. Hartmann M, Heumann R, Lessmann V. Synaptic secretion of BDNF after high-frequency stimulation of glutamatergic synapses. *Embo j* **20**, 5887-5897 (2001).

88. McIntyre RS*, et al.* Synthesizing the Evidence for Ketamine and Esketamine in Treatment-Resistant Depression: An International Expert Opinion on the Available Evidence and Implementation. *Am J Psychiatry* **178**, 383-399 (2021).

89. Anderson MC*, et al.* Trans-synaptic molecular context of NMDA receptor nanodomains. *Nat Commun* **16**, 7460 (2025).

90. Henry FE*, et al.* Retrograde changes in presynaptic function driven by dendritic mTORC1. *J Neurosci* **32**, 17128-17142 (2012).

91. Nowak L, Bregestovski P, Ascher P, Herbet A, Prochiantz A. Magnesium gates glutamate-activated channels in mouse central neurones. *Nature* **307**, 462-465 (1984).

92. Espinosa F, Kavalali ET. NMDA receptor activation by spontaneous glutamatergic neurotransmission. *J Neurophysiol* **101**, 2290-2296 (2009).

93. Yuzaki M*, et al.* Mode of blockade by MK-801 of N-methyl-D-aspartate-induced increase in intracellular Ca2+ in cultured mouse hippocampal neurons. *Brain Res* **517**, 51-56 (1990).

94. Gideons ES, Kavalali ET, Monteggia LM. Mechanisms underlying differential effectiveness of memantine and ketamine in rapid antidepressant responses. *Proc Natl Acad Sci U S A* **111**, 8649-8654 (2014).

95. Atasoy D*, et al.* Spontaneous and evoked glutamate release activates two populations of NMDA receptors with limited overlap. *J Neurosci* **28**, 10151-10166 (2008).

96. Duman RS, Aghajanian GK, Sanacora G, Krystal JH. Synaptic plasticity and depression: new insights from stress and rapid-acting antidepressants. *Nat Med* **22**, 238-249 (2016).

97. Lin PY, Ma ZZ, Mahgoub M, Kavalali ET, Monteggia LM. A synaptic locus for TrkB signaling underlying ketamine rapid antidepressant action. *Cell Rep* **36**, 109513 (2021).

98. Perez-Otano I*, et al.* Assembly with the NR1 subunit is required for surface expression of NR3A-containing NMDA receptors. *J Neurosci* **21**, 1228-1237 (2001).

99. Sasaki YF*, et al.* Characterization and comparison of the NR3A subunit of the NMDA receptor in recombinant systems and primary cortical neurons. *J Neurophysiol* **87**, 2052-2063 (2002).

100. Al-Hallaq RA, Jarabek BR, Fu Z, Vicini S, Wolfe BB, Yasuda RP. Association of NR3A with the N-methyl-D-aspartate receptor NR1 and NR2 subunits. *Mol Pharmacol* **62**, 1119-1127 (2002).

101. Nilsson A*, et al.* Analysis of NR3A receptor subunits in human native NMDA receptors. *Brain Res* **1186**, 102-112 (2007).

102. Miller OH*, et al.* GluN2B-containing NMDA receptors regulate depression-like behavior and are critical for the rapid antidepressant actions of ketamine. *Elife* **3**, e03581 (2014).

103. Savtchouk I, Di Castro MA, Ali R, Stubbe H, Luján R, Volterra A. Circuit-specific control of the medial entorhinal inputs to the dentate gyrus by atypical presynaptic NMDARs activated by astrocytes. *Proc Natl Acad Sci U S A* **116**, 13602-13610 (2019).

104. Sadat-Shirazi MS*, et al.* NMDA receptors of blood lymphocytes anticipate cognitive performance variations in healthy volunteers. *Physiol Behav* **201**, 53-58 (2019).

105. Kleindienst T, Winnubst J, Roth-Alpermann C, Bonhoeffer T, Lohmann C. Activity-dependent clustering of functional synaptic inputs on developing hippocampal dendrites. *Neuron* **72**, 1012-1024 (2011).

106. Makino H, Malinow R. Compartmentalized versus global synaptic plasticity on dendrites controlled by experience. *Neuron* **72**, 1001-1011 (2011).

107. Druckmann S*, et al.* Structured synaptic connectivity between hippocampal regions. *Neuron* **81**, 629-640 (2014).

108. Kvist T, Greenwood JR, Hansen KB, Traynelis SF, Bräuner-Osborne H. Structure-based discovery of antagonists for GluN3-containing N-methyl-D-aspartate receptors. *Neuropharmacology* **75**, 324-336 (2013).

109. Zhu Z*, et al.* Negative allosteric modulation of GluN1/GluN3 NMDA receptors. *Neuropharmacology* **176**, 108117 (2020).

110. Arellano JI, Benavides-Piccione R, Defelipe J, Yuste R. Ultrastructure of dendritic spines: correlation between synaptic and spine morphologies. *Front Neurosci* **1**, 131-143 (2007).

111. Patterson M, Yasuda R. Signalling pathways underlying structural plasticity of dendritic spines. *Br J Pharmacol* **163**, 1626-1638 (2011).

112. Wenzel HJ, Cole TB, Born DE, Schwartzkroin PA, Palmiter RD. Ultrastructural localization of zinc transporter-3 (ZnT-3) to synaptic vesicle membranes within mossy fiber boutons in the hippocampus of mouse and monkey. *Proc Natl Acad Sci U S A* **94**, 12676-12681 (1997).

113. Milner TA, Waters EM, Robinson DC, Pierce JP. Degenerating processes identified by electron microscopic immunocytochemical methods. *Methods Mol Biol* **793**, 23-59 (2011).

114. Williams RA, Johnson KW, Lee FS, Hemmings HC, Jr., Platholi J. A Common Human Brain-Derived Neurotrophic Factor Polymorphism Leads to Prolonged Depression of Excitatory Synaptic Transmission by Isoflurane in Hippocampal Cultures. *Front Mol Neurosci* **15**, 927149 (2022).

115. Paxinos G, Franklin KBJ. *Paxinos and Franklin's the mouse brain in stereotaxic coordinates*, 4th edn. Elsevier Academic Press (2013).

116. Park H, Popescu A, Poo MM. Essential role of presynaptic NMDA receptors in activity-dependent BDNF secretion and corticostriatal LTP. *Neuron* **84**, 1009-1022 (2014).

117. Peters A, Palay S, Webster H. *The fine structure of the nervous system*. Oxford UP (1991).

118. Pierce JP, Kelter DT, McEwen BS, Waters EM, Milner TA. Hippocampal mossy fiber leu-enkephalin immunoreactivity in female rats is significantly altered following both acute and chronic stress. *J Chem Neuroanat* **55**, 9-17 (2014).

119. Shimojo M*, et al.* SNAREs Controlling Vesicular Release of BDNF and Development of Callosal Axons. *Cell Rep* **11**, 1054-1066 (2015).

120. Jiang Y, Wang Z, Scheuring S. A structural biology compatible file format for atomic force microscopy. *Nat Commun* **16**, 1671 (2025).

121. Garcia SB, Schlotter AP, Pereira D, Recupero AJ, Polleux F, Hammond LA. RESPAN: A Deep Learning Pipeline for Accurate and Automated Restoration, Segmentation, and Quantification of Dendritic Spines. *bioRxiv*, (2025).

122. Libé-Philippot B*, et al.* Synaptic neoteny of human cortical neurons requires species-specific balancing of SRGAP2-SYNGAP1 cross-inhibition. *Neuron* **112**, 3602-3617.e3609 (2024).

123. Isensee F, Jaeger PF, Kohl SAA, Petersen J, Maier-Hein KH. nnU-Net: a self-configuring method for deep learning-based biomedical image segmentation. *Nat Methods* **18**, 203-211 (2021).